Bistatic Scattering at a Cylindrical Cavity

K. W. Kark

Inst. f. Hochfrequenztechnik, DFVLR - Deutsche Forschungs- und Versuchsanstalt für Luft- und Raumfahrt, D-8031 Oberpfaffenhofen, F.R. Germany.

Abstract

An approximate high-frequency analysis is presented for calculating the far-zone fields scattered by a perfectly-conducting, open-ended, semi-infinite circular cylinder. Inside this oversized hollow waveguide ($k_0 a \gg 1$) which is illuminated by an external electromagnetic plane wave a planar impedance boundary is located at $z = -L$. The permittivity in the regions A and B is ε_0, whereas region C contains a homogeneous dielectric ε_1. A hybrid field description using rays and modes yields new bistatic scattering matrices as a generalization of the former monostatic theory.

1. Introduction

This paper considers the radar problem of bistatic scattering of plane electromagnetic waves at a semi-infinite circular cylinder. Structures of cylindrical shape which are used for jet air intakes and satellites are important components for the radar analysis of complicated bodies using the geometrical theory of diffraction (GTD, *Keller* [7]). Hitherto existing ray-optical investigations only deal with the monostatic backscattering from a cylindrical cavity (*Pathak et al* [9]).

For oversized waveguides with large cross section ($k_0 a \gg 1$) the boundary value problem can be solved approximately with a hybrid field description. The effects of aperture coupling and rim diffraction are treated by a ray-optical approach, and the wave propagation inside the cylinder is investigated using an eigenmode expansion. The currents on the outer surface of the cylinder may be neglected, since the considered source and observer directions are restricted to $0° \le \vartheta_i, \vartheta_s \le 60°$ (see Figure 1).

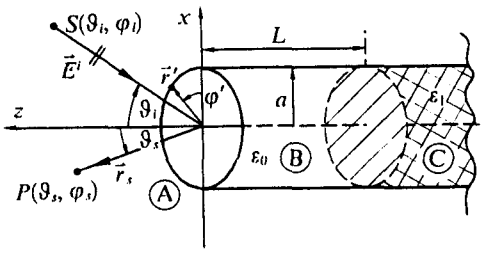

Figure 1. **Bistatic scattering at a semi-infinite circular cylinder** with dielectric loading. The source $S(\vartheta_i, \varphi_i)$ and the observer $P(\vec{r}_s)$ are located in the far zone of the circular edge of the aperture. The allowable angular region for the approximate theory is about $0° \le \vartheta_i, \vartheta_s \le 60°$.

2. Scattering-matrix description

To solve the overall scattering problem the continuity at both interfaces I and II between the regions A-B and B-C must be assured. The far field is described via the scattering matrix [S] which is defined for a linear polarization basis $\vec{E}^s = E^s_\vartheta \hat{\vartheta}_s + E^s_\varphi \hat{\varphi}_s$ (unit vectors are indicated by a hat) and harmonic time dependence ($e^{j\omega t}$) :

$$\vec{E}^s(\vec{r}_s) = [S] \frac{e^{-j k_0 r_s}}{k_0 r_s} \vec{E}^i(\vec{r} = \vec{0}) \quad . \tag{1}$$

To represent the incident wave at an arbitrary point $P(\vec{r})$ the following ansatz is made:

$$\vec{E}^i(\vec{r}) = \left(E^i_\vartheta \hat{\vartheta}_i + E^i_\varphi \hat{\varphi}_i \right) e^{j k_0 \hat{r}_i \cdot \vec{r}} \quad . \tag{2}$$

The wave number is $k_0 = 2\pi / \lambda_0 = \omega\sqrt{\mu_0 \varepsilon_0}$. The complex phasors E^i_ϑ and E^i_φ determine the polarization of the incident plane wave. In the following only the azimuthal angle of incidence $\varphi_i = 0°$ is considered; this means no restriction since the scattering arrangement is rotationally symmetrical around the z-axis. The plane of incidence defined by $\hat{r}_i$ and $\hat{z}$ is thus identical to the x-z-plane of the spherical coordinate system (Figure 1).

Having defined appropriate reflection and transmission matrices (see Figure 2) the total bistatic scattering matrix [S] can be given (*Pathak et al* [8]):

$$[S] = [R_A] + [H] \tag{3}$$

with the rim-diffraction matrix $[R_A]$ and the hollow-waveguide matrix $[H]$:

$$[H] = [T_A] \left([I] - [M_B] [R'_B] \right)^{-1} [M_B] [T_B] \quad ,$$

which contains the interior cavity effects arising from all interactions between forward and backward traveling waves.

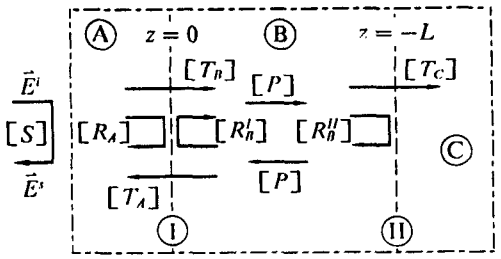

Figure 2. **The total scattering matrix** [S] is decomposed into reflection and transmission matrices arising from the continuity conditions at the interfaces I and II.

It can be shown that $[R_A]$ only contains real elements, while $[H]$ is generally complex. The diagonal matrix $[M_B] = [P][R''_B][P]$ consists of the phase-delay matrix $[P]$ and the interior reflection matrix $[R''_B]$. $[I]$ is the identity matrix. It now remains to find explicit expressions for the matrices $[R_A]$ and $[H]$ to complete the calculation in Eq. (3). The edge-diffraction matrix $[R_A]$ is computed via the equivalent current method (ECM) which is based on the geometrical theory of diffraction (GTD). Electric and magnetic equivalent line currents $I_e \hat{\varphi}'$ and $I_m \hat{\varphi}'$ are derived along the circular edge of the aperture of the waveguide. Their free-space radiation behaviour is found via an integral representation of the field equations:

$$\vec{E}^s_{R_A}(\vec{r}_s) = j k_0 a \frac{e^{-j k_0 r_s}}{4\pi r_s} \int_0^{2\pi} \left[Z_0 \hat{r}_s \times (\hat{r}_s \times \hat{\varphi}') I_e(\varphi') + \right.$$

$$\left. + \hat{r}_s \times \hat{\varphi}' I_m(\varphi') \right] e^{j k_0 \hat{r}_s \cdot \vec{r}'} d\varphi' = [R_A] \frac{e^{-j k_0 r_s}}{k_0 r_s} \vec{E}^i(\vec{r} = \vec{0})$$

with $Z_0 = 1 / Y_0 = \sqrt{\mu_0 / \varepsilon_0}$ as the characteristic impedance of the free space. Via the method of stationary

phase (*Erdélyi* [4]) this bistatic diffraction integral can approximately be reduced for $k_0 a \gg 1$ to integrals of the Sommerfeld type, leading to Bessel function solutions (for details see *Kark* [5] and [6]). The reflection matrix $[R_B']$ is similarly derived applying the ECM. The transmission matrices $[T_A]$ and $[T_B]$ (*Altintas* [1]) are computed using Kirchhoff 's aperture integral technique (physical optics - PO) together with the Ufimtsev edge diffraction method (physical theory of diffraction - PTD). The matrix $[M_B]$ simply results from standard waveguide modal theory. Here, only the special case of a metallic plate (short circuit) located at $z = -L$ inside the waveguide can be considered. For $\mathrm{Im}\{\varepsilon_1\} \to -\infty$ we simply get $[R_B''] = -[I]$, otherwise $[R_B'']$ contains the modal reflection coefficients depending on the permittivity ε_1.

An important advantage of the performed computations is the analytical closed-form representation of all diffraction integrals and scattering matrices. Thus, in contrast to purely numerical methods, the computational effort only weakly increases with the actual waveguide dimensions, even for very large cross sections ($k_0 a \gg 1$). In the monostatic special case ($\vartheta_s = \vartheta_i$, $\varphi_s = \varphi_i$) *Pathak et al* [9] made comparisons with the exact Wiener-Hopf solution for the diffraction at a semi-infinite circular cylinder and they found a good agreement with their approximate solution in the whole range of aspect angles ($0° \leq \vartheta_s \leq 60°$).

2.1 Polarization effects

Since the cylindrical scatterer is rotationally symmetrical one only needs to consider the azimuthal angle of incidence $\varphi_i = 0°$ (see Figure 1) without loss of generality. Thus a linear (V-H) polarization basis can be built up very simply: $E_V = E_\vartheta$ and $E_H = E_\varphi$. Starting from the complex far-zone scattering matrix $[S]$

$$[S] = \begin{pmatrix} S_{\vartheta\vartheta} & S_{\vartheta\varphi} \\ S_{\varphi\vartheta} & S_{\varphi\varphi} \end{pmatrix} = \begin{pmatrix} S_{VV} & S_{VH} \\ S_{HV} & S_{HH} \end{pmatrix} \tag{4}$$

which holds for linear (V-H) polarization vectors, the scattering matrix $[S_C]$ for a circular (LHC-RHC) polarization basis is obtained after two matrix multiplications (*Cloude* [3]):

$$[S_C] = [U][S][U]^{-1} = \begin{pmatrix} S_{LL} & S_{LR} \\ S_{RL} & S_{RR} \end{pmatrix}$$

with the unitary matrix

$$[U] = \frac{1}{\sqrt{2}} \begin{pmatrix} 1 & -j \\ 1 & j \end{pmatrix} .$$

The particular scattering coefficients are:

$$S_{LL} = [S_{\vartheta\vartheta} + S_{\varphi\varphi} + j(S_{\vartheta\varphi} - S_{\varphi\vartheta})]/2 \tag{5}$$

$$S_{RR} = [S_{\vartheta\vartheta} + S_{\varphi\varphi} - j(S_{\vartheta\varphi} - S_{\varphi\vartheta})]/2 \tag{6}$$

$$S_{RL} = [S_{\vartheta\vartheta} - S_{\varphi\varphi} + j(S_{\vartheta\varphi} + S_{\varphi\vartheta})]/2 \tag{7}$$

$$S_{LR} = [S_{\vartheta\vartheta} - S_{\varphi\varphi} - j(S_{\vartheta\varphi} + S_{\varphi\vartheta})]/2 . \tag{8}$$

3. Scattering diagrams

To demonstrate the scattering behaviour at a semi-infinite circular cylinder with an interior short circuit at $z = -L$ the spatial far-zone distribution of the radial energy-flux density of the scattered field is considered:

$$P_r^s = \frac{Y_0}{2} |\vec{E}^s|^2 = \frac{Y_0}{2} \left(|E_\vartheta^s|^2 + |E_\varphi^s|^2 \right) .$$

The radiation characteristic C is then defined:

$$C(\vartheta_i, \varphi_i; \vartheta_s, \varphi_s) = \lim_{k_0 r_s \to \infty} (k_0 r_s)^2 \frac{|\vec{E}^s|^2}{|\vec{E}^i|^2} , \tag{9}$$

leading to the radar cross section (normalized to λ_0^2)

$\sigma = 10 \lg C$ dB .

A vertically polarized incident plane wave implies $E_\varphi^i = 0$ for $\varphi_i = 0°$ and one obtains from Eq. (9) the scattering characteristic C_V using the Eqs. (1), (2) and (4):

$$C_V = |S_{\vartheta\vartheta}|^2 + |S_{\varphi\vartheta}|^2 . \tag{10}$$

In an analogous manner is $E_\vartheta^i = 0$ for an incident horizontally polarized plane wave and one gets:

$$C_H = |S_{\varphi\varphi}|^2 + |S_{\vartheta\varphi}|^2 . \tag{11}$$

An incident plane wave with left or right handed circular polarization yields the radiation characteristic using the Eqs. (5) to (8):

$$\begin{aligned} C_{LHC} &= |S_{LL}|^2 + |S_{RL}|^2 \\ C_{RHC} &= |S_{RR}|^2 + |S_{LR}|^2 . \end{aligned} \tag{12}$$

3.1 Bistatic radar cross section

For a normalized waveguide radius $k_0 a = 11$ ($2a = 3.5\,\lambda_0$) with an inner short circuit located at $kL = 50$ the following three-dimensional polar plots show the spatial distribution of the radial energy-flux density of the scattered field in the bistatic scattering problem, i.e. the bistatic radar cross section σ. A logarithmic scale with a dynamic range of -40 dB to 0 dB was used. The direction of incidence of the plane wave is indicated by $\varphi_i = 0°$ and $\vartheta_i = 0°$ or $\vartheta_i = 22°$, respectively. The scattering diagram is only displayed in the range $0° \leq \vartheta_s \leq 60°$. It can be shown that about 75% of the energy, which has entered the oversized waveguide through the aperture, is then re-radiated into the aforementioned 60° conical region.

For an incident plane wave of linear or circular polarization the corresponding radar cross sections σ_V, σ_H, σ_{LHC} and σ_{RHC} are shown in Figure 3. Relative to the plane of incidence (x-z-plane, for $\varphi_i = 0°$) there exist some remarkable symmetry relations. σ_V and σ_H are always symmetrical relative to the x-z-plane. For *axial* incidence ($\vartheta_i = 0°$) σ_H is obtained from σ_V after a rotation of 90° around the z-axis, and in the circular polarized case a rotationally symmetrical diagram is obtained with $\sigma_{LHC} = \sigma_{RHC}$. For *oblique* incidence ($\vartheta_i > 0°$) the LHC and RHC cases behave different. The diagrams are unsymmetrical and we obtain σ_{RHC} from σ_{LHC} after mirroring with respect to the x-z-plane.

3.2 Monostatic radar cross section

In the monostatic case ($\vartheta_s = \vartheta_i$, $\varphi_s = \varphi_i$) the radiation characteristic does not depend on the azimuthal angle φ_s, i.e. $C = C(\vartheta_s)$. For a normalized hollow-waveguide radius $k_0 a = 21$ ($2a = 6.685\,\lambda_0$) with an inner short circuit located at $kL = 20\pi$ Figure 4 shows the monostatic radar cross section σ for different polarizations (V, H, C) of the incident wave. The left and right handed circular case (LHC, RHC) behave identical in monostatic scattering. The corresponding results completely agree with older computations (*Altintas et al* [2]) and indicate that the scattering contribution coming from the cavity $[H]$ is much stronger than the rim-diffracted part $[R_A]$. Only for small apertures $[R_A]$ is expected to give a relevant contribution to the total scattering matrix $[S]$.

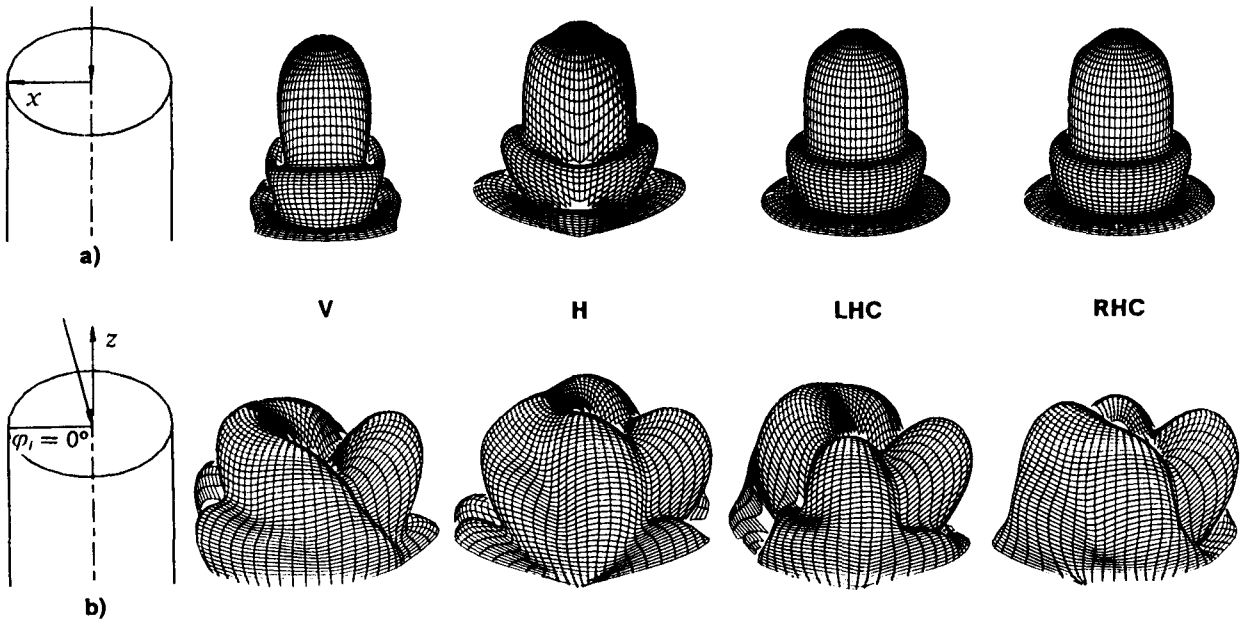

Figure 3. **Bistatic radar cross section** σ_V , σ_H, σ_{LHC} and σ_{RHC} (see the Eqs. (10) to (12) with $\sigma = 10 \lg C$ dB) *for an incident linearly or circularly polarized plane wave. The diameter 2a of* the circular cylinder is 3.5 free-space wavelengths ($k_0 a = 11$) and a metallic plate (short circuit) is located at $kL = 50$ inside the waveguide. Two different situations are displayed: **a)** axial incidence ($\vartheta_i = 0°$) and **b)** oblique incidence ($\vartheta_i = 22°$).

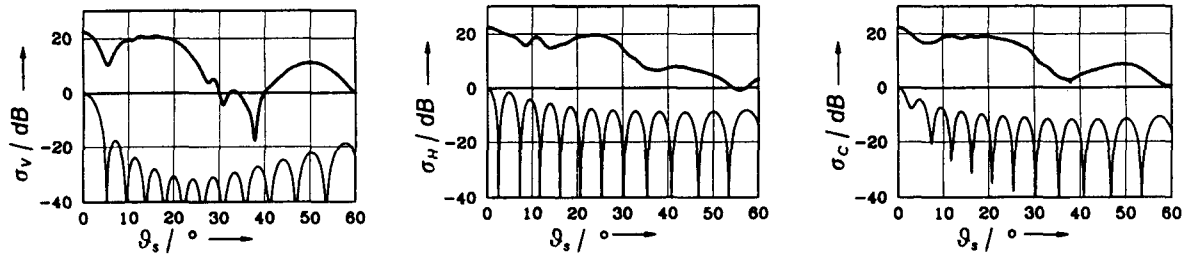

Figure 4. **Monostatic radar cross section** σ_V , σ_H and σ_C *(see the Eqs. (10) to (12) with* $\sigma = 10 \lg C$ dB) *for* an incident linearly or circularly polarized plane wave. The diameter 2a of the circular cylinder is 6.685 free-space wavelengths ($k_0 a = 21$) and a metallic plate (short circuit) is located at $kL = 20\,\pi = 62.832$ inside the waveguide. A logarithmic scale with a dynamic range of -40 dB to 0 dB was used for the rim-diffracted part $[R_A]$ (lower curves). The total backscattered signal connected with $[S]$ *(upper curves) indicates the strongly dominant effect of the cavity* term $[H]$, i.e. $[S] \approx [H]$ for $k_0 a \gg 1$ (see Eq. (3)).

4. Concluding remarks

This paper considered the radar problem of bistatic scattering of plane electromagnetic waves at a semi-infinite circular cylinder. The diffraction at the circular rim of the aperture and the interior cavity effects were investigated. An efficient hybrid approach using ray-optical high frequency solutions and modal expansion methods was described. Thus, new bistatic scattering matrices as a generalization of the former monostatic theory could be derived. The field of application of the computations is restricted to the angular domain $0° \leq \vartheta_{i,s} \leq 60°$. Of special interest is a future investigation of the scattered field in the direct near-zone of the aperture of the waveguide. To improve the precision of the performed approximate computations higher oder terms can be introduced which arise from multiply diffracted rays across the aperture.

5. References

[1] Altintas, A.: *Electromagnetic Scattering from a Class of Open-Ended Waveguide Discontinuities.* Ph.D. diss., Ohio State Univ., Dept. Electr. Eng., Columbus (1986).

[2] Altintas, A.; Pathak, P.H.; Liang, M.-C.: *A Selective Modal Scheme for the Analysis of EM Coupling into or Radiation from Large Open-Ended Waveguides.* IEEE Trans. Ant. Prop., vol. AP-36 (1988), 84-96.

[3] Cloude, S.R.: *Polarimetric Techniques in Radar Signal Processing.* Microwave J. (1983), 119-127.

[4] Erdélyi, A.: *Asymptotic Expansions.* Dover Publ., New York (1956), 51-56.

[5] Kark, K.W.: *Theoretische Untersuchungen zur bistatischen Streuung an einer kreisförmigen Kante.* Nat. U.R.S.I. Conf., F.R. Germany, Proc.: Kleinheubacher Berichte, vol. 32 (1988), 207-218.

[6] Kark, K.W.: *Equivalent Current Method for Bistatic Scattering at a Circular Edge.* 3rd Int. IGTE Symposium on Numerical Field Calculation in Electr. Eng., Proc., TU Graz, Austria (1988), 64-71.

[7] Keller, J.B.: *Geometrical Theory of Diffraction.* J. Opt. Soc. Am., vol. JOSA-52 (1962), 116-130.

[8] Pathak, P.H.; Chuang, C.W.; Liang, M.C.: *Near Field Scattering by Rectangular and Circular Inlet Configurations.* Final Report 716495-2, Ohio State Univ., Dept. Electr. Eng., Columbus (1985).

[9] Pathak, P.H.; Huang, C.C.; Lai, C.Y.; Moffat, D.L.: *Analysis of Electromagnetic Backscatter from an Inlet Cavity Configuration.* Final Report 712661-4, Ohio State Univ., Dept. Electr. Eng., Columbus (1983).